Drug Design, Development and Therapy

Dovepress
Taylor & Francis Group

Open Access Full Text Article

ORIGINAL RESEARCH

Modified Sijunzi Decoction Inhibits Pancreatic Cancer Progression and Improves Immune Suppression: Network Pharmacology and Experimental Validation

Yuan Zhang[1,2], Linjie Ruan[1,2], Xin Li[1,2], Waimei Si[1,2], Peiwen Yang[1,2], He Ba[1,2], Zhen Chen[1,2]

[1]Department of Integrative Oncology, Fudan University Shanghai Cancer Center, Shanghai, People's Republic of China; [2]Department of Oncology, Shanghai Medical College, Fudan University, Shanghai, People's Republic of China

Correspondence: Zhen Chen, Department of Integrative Oncology, Fudan University Shanghai Cancer Center, No. 270 Dongan Road, Xuhui District, Shanghai, 200032, People's Republic of China, Email zchenzl@fudan.edu.cn

Purpose: This study aimed to assess the effectiveness of Modified Sijunzi Decoction (MSJZD) in pancreatic cancer (PC) treatment. Molecular mechanisms were elucidated and active ingredients were screened using network pharmacology, RNA sequencing, and in vivo experiments, providing a scientific foundation for the clinical application of MSJZD in PC treatment.

Methods: We established an orthotopic PC mouse model and treated it with different MSJZD concentrations to evaluate its efficacy. Ultra-high-performance liquid chromatography Q-Exactive mass spectrometry was used to identify MSJZD components. Through integrated pharmacology analyses, the active ingredients, core targets, and signaling pathways were determined, and active ingredients targeting the core targets were screened using molecular docking simulations. RNA-sequencing analyses of the molecular mechanism of MSJZD in PC treatment were verified using immunohistochemistry and Western blotting. A multiplex immunofluorescence assay was used to detect macrophage and $CD8^+$ T cell infiltration levels.

Results: MSJZD effectively inhibited the growth of orthotopic pancreatic tumors in mice via JAK1-STAT3 pathway and reduced Ki-67 expression, with no discernible toxicity to the liver and kidneys. MSJZD relieved immunosuppression by decreasing M2 macrophage infiltration, increasing $CD8^+$ T cell infiltration, and lowering the expression of immunosuppressive cytokines (interleukins 10 and 6). Network pharmacology analysis revealed that EGFR, SRC, AKT1, and STAT3 were the core MSJZD targets in PC treatment. Molecular docking revealed a strong binding affinity between wedelolactone and its core target proteins (EGFR, SRC, AKT1).

Conclusion: MSJZD is a safe and effective decoction for PC that exerts anti-tumor effects by inhibiting JAK1-STAT3 pathway and improving immunosuppressive microenvironment by reducing M2 macrophage infiltration and increasing $CD8^+$ T cell infiltration. This study reveals MSJZD therapeutic potential and offers a reference for further research.

Keywords: Traditional Chinese Medicine, integrated pharmacology, macrophage polarization, molecular mechanism, Pancreatic Cancer

Introduction

Pancreatic cancer (PC) has shown an increasing trend in both global incidence and mortality rates. According to data released by the American Cancer Society in 2025, the 5-year survival rate for PC is only 13%.[1] Most patients (50–55%) are diagnosed with metastatic disease, and standard chemotherapy with 5-fluorouracil, irinotecan, leucovorin, and oxaliplatin (FOLFIRINOX) or single-agent gemcitabine fails to confer a substantial survival advantage.[2–4] Consequently, there is an acute need for target screening and identification of novel agents that induce disease remission and symptom alleviation.

Traditional Chinese Medicine has extensive experience in PC treatment. The Modified Sijunzi Decoction (MSJZD) is an empirical formulation derived from the Sijunzi Decoction (SJZD) composed of *Atractylodes macrocephala* Koidz.

Received: 27 March 2025
Accepted: 20 September 2025
Published: 2 October 2025

(Baizhu), *Poriacocos* (Schw). Wolf (Fuling), *Codonopsis pilosula* (Fanch). Nannf. (Dangshen), *Glycyrrhiza uralensis* Fisch. (Gancao), *Rhodiola crenulate* (Hook. f. et Thoms)., H. Ohba (Hongjingtian), and *Dioscorea opposita* Thunb. (Shanyao). All these herbs belong to "food and medicine homology" (FMH) Chinese medicine, defined as substances associated with pharmacological and nutritional properties, containing fundamentally non-toxic active ingredients suitable for extended consumption.[5] FMH substances have excellent potential in tumor therapy and adjuvant tumor treatment as they minimize adverse reactions associated with cancer therapy.[6,7] Contemporary pharmacological research revealed that SJZD can enhance immune function,[8] promote metabolism,[9] and inhibit digestive tract tumors.[10–12] *Rhodiola crenulate* extracts and active compounds have been reported to have anti-inflammatory effects,[13] initiate the programmed death of tumor cells, and regulate the functionality of immune cells.[14,15] Additionally, these substances are capable of inducing apoptosis and promoting protective autophagy in gastric cancer tissues.[16] *Dioscorea opposita* Thunb. contains abundant bioactive compounds, which have been found to exert anti-oxidant effects,[17] enhance immunomodulatory activity of macrophages and T cells,[18–20] and inhibit breast cancer cell activity, nasopharyngeal carcinoma, and hepatoma cell proliferation.[21,22] These findings motivated us to elucidate the efficacy of diverse ingredients within Modified Sijunzi Decoction (MSJZD) in ameliorating symptoms, potentially inhibiting tumor growth, and uncovering the pharmacological mechanisms of anti-PC effects.

Network pharmacology has been extensively applied to elucidate the associations between drugs and pathological conditions at both the molecular and systemic levels, and offers a comprehensive portrayal of the characteristics and underlying mechanisms governing the multi-component, multi-pathway, and multi-target effects exerted by oral herbal formulas. In this study, we investigated the anti-tumor potential of MSJZD in an orthotopic PC mouse model and evaluated its safety. We screened core targets and potential active ingredients using network pharmacology, combining RNA-sequencing (RNA-seq) analysis to explore the molecular mechanisms of MSJZD in PC treatment.

Materials and Methods

Preparation of MSJZD

MSJZD is composed of six Chinese medicine granules purchased from Guangdong Yifang Pharmaceutical Co., Ltd. (Foshan, China), and their contents are presented in Table 1. The administration concentrations for C57BL/6 mice were calculated for MSJZD high-dose group (MSJZD-H) and MSJZD low-dose group (MSJZD-L) based on the daily clinical dose for a 70 kg adult, using body surface area conversion method.[23] The Chinese medicine granules were dissolved in normal saline (NS) and then stored at 4°C after cooling.

Establishment of Pancreatic Orthotopic Tumor Models and Treatment Interventions

Pancreatic orthotopic tumor models were established using 6-week-old male C57BL/6 mice procured from Shanghai Jihui Laboratory Animal Care Co. Ltd (Shanghai, China). The Experimental Animal Welfare and Ethics Committee of Fudan University Experimental Animal Center approved the animal experimental protocols used in this study. The animal

Table 1 The Proportion of the MSJZD

Chinese Name	Plant Name	Proportion (g) of MSJZD-H	Proportion (g) of MSJZD-L
Baizhu	*Atractylodes macrocephala* Koidz.	30	10
Fuling	*Poriacocos* (Schw.) Wolf	30	10
Dangshen	*Codonopsis pilosula* (Franch.) Nannf.	30	10
Gancao	*Glycyrrhiza uralensis* Fisch.	10	3
Hongjingtian	*Rhodiola crenulate* (Hook. f. et Thoms.) H. Ohba	30	10
Shanyao	*Dioscorea opposita* Thunb.	30	10

experiments adhered to the "3R" basic principles of experimental animal welfare recognized internationally, namely replacement, reduction, and refinement. Mice were anesthetized with a combination of tiletamine hydrochloride and zolazepam hydrochloride for injection at a dose of 50 mg/kg, and xylazine at a dose of 10 mg/kg. Panc02 cells were mixed in a 1:1 ratio with Matrigel and 30 μL cell suspension (1×10^6 cells) were injected under the pancreatic envelope of anesthetized mice. After 7 d, tumor formation was confirmed, and the mice were randomized into NS (n=12), MSJZD-L (n=12), and MSJZD-H (n=12) groups. The latter two groups were gavaged with different MSJZD concentrations, and the NS group was administered an equal volume of saline. After 21 days of treatment, tumors were detected using an IVIS Spectrum (PerkinElmer, USA), and all mice were euthanized by professionals using the carbon dioxide inhalation method.

Cell Lines and Culture

Mouse PC cell line Panc02 was purchased from Pricella (CL-0736, Wuhan Pricella Biotechnology, Wuhan, China) and cultured in high-glucose Dulbecco's modified Eagle's medium (DMEM, L110KJ, Basal Media Technologies, Shanghai, China) supplemented with 1% penicillin/streptomycin/amphotericin B (PSA; S120JV, Basal Media Technologies) and 10% fetal bovine serum (FBS; F1093, Sigma-Aldrich, Germany). The cells were maintained and incubated under sterilized and humidified conditions with 5% CO_2 at 37°C.

Ultra-High-Performance Liquid Chromatography Q-Exactive Mass Spectrometry (UHPLC-Q-Exactive-MS) Analysis

Drug component analysis was performed by Shanghai OE Biotech Co., Ltd (Shanghai, China). An ACQUITY UPLC I-Class Plus coupled with a Q-Exactive mass spectrometer was used for metabolic profiling in positive and negative electrospray ionization modes. An ACQUITY UPLC HSS T3 column was used with gradient elution (water/acetonitrile with 0.1% formic acid, 5% B at 0.01 min to 100% B at 14–15 min then back to 5%). Chromatographic conditions were as follows: flow rate, 0.35 mL/min; column temp, 45°C; sample storage, 4°C; injection volume, 5 μL.

MSJZD Active Component Screening and Potential Target Prediction

The Simplified Molecular Input Line Entry System (SMILES) structures were entered into the SwissADME database (http://www.swissadme.ch/) to screen the active ingredients. The screening criteria were: molecular weight (MW) < 500, high oral bioavailability (OB), hydrogen bond acceptors (Hacc) ≤ 10, hydrogen bond donors (Hdon) ≤ 5, and octanol-water partition coefficient (LogP) ≤ 5. Subsequently, the SMILES structures were imported into the SwissTargetPrediction (http://www.swisstargetprediction.ch/) and TargetNet databases (http://targetnet.scbdd.com/home/index/) to predict the potential targets of the active ingredients in MSJZD.

MSJZD Target Identification for PC Treatment

Target genes associated with PC were identified from the Therapeutic Target Database (TTD, http://db.idrblab.net), the Cancer Genome Atlas (TCGA, https://www.cancer.gov/ccg/research/genome-sequencing/tcga), the genome annotation platform of the human gene database (GeneCards, https://www.genecards.org), and the Online Mendelian Inheritance in Man database (OMIM, http://www. omim.org). Duplicates were merged and removed from the genes collected from the above-mentioned databases to obtain the disease targets of PC. Finally, the Venn platform (https://www.bioinformatics.com.cn) was used to identify targets of MSJZD for PC treatment.

Protein-Protein Interaction (PPI) Network Construction and Core Gene Identification

The intersection of the MSJZD and PC targets was imported into the STRING database (https://cn.string-db.org/). The database was set to the highest confidence level (0.900) to construct the PPI network. The TSV file downloaded from the STRING database was later input into Cytoscape 3.7.0. Three rounds of screening were performed using the medians of the degree centrality (DC), betweenness centrality (BC), closeness centrality (CC), eigenvector centrality (EC), information (IC), local average connectivity (LAC), and Network (NC) values in CytoNCA to identify the core genes (Table 2).

Table 2 Filter Conditions of CytoNCA

	Fliter1	Fliter2	Fliter3
DC	6	20	36
BC	118.944	1466.6	4214.5
CC	0.047	0.064	0.112
EC	0.006	0.076	0.213
IC	2.950	4.095	4.47
LAC	2	6.4	8.667
NC	3.25	9.244	17.455

Gene Ontology (GO) and Kyoto Encyclopedia of Genes and Genomes (KEGG) Pathway Enrichment Analyses

GO and KEGG pathway enrichment analyses were carried out using the Metascape database (https://metascape.org/gp/). The data were visualized using a bioinformatics platform (https://www.bioinformatics.com.cn/).

Molecular Docking

The 3D structures of epidermal growth factor receptor (EGFR; 1m17), oncogene Src (SRC; 1y57), AKT serine/threonine kinase 1 (AKT1; 3cqw), and signal transducer and activator of transcription 3 (STAT3; 6njs) were downloaded from the Protein Data Bank (http://www.rcsb.org/). Using PyMOL 3.0.4, water and ligands were removed from the protein. Subsequently, AutoDockTools were employed to add hydrogen and balance charges. Both the receptor protein and ligand were converted into pdbqt format. Molecular docking between the receptor protein and ligand was performed using AutoDock Vina 1.1.2, with a semi-flexible docking model, and results were analyzed using Protein–Ligand Interaction Profiler. Docking results were visualized using PyMOL software. Molecular docking parameters of the core targets are listed in Table S1. The binding energies between the proteins and ingredients are listed in Table S2. Screening was performed using the average binding energy values from the molecular docking of three positive drugs with each target as the threshold.[24] Information on positive drugs and their binding energies with targets are listed in Table S3.

RNA-Seq

Tumor tissue was excised from the mice and immediately frozen in liquid nitrogen. Total RNA was extracted from the tumor tissue using the Universal RNA Extraction CZ Kit (RNC643, ONREW) according to the manufacturer's instructions. RNA quantity was analyzed using Qubit 4.0 (Thermo Fisher Scientific, USA), and RNA quality was examined using electrophoresis on a denaturing agarose gel. RNA libraries were prepared using the VVAHTS® Universal V8 RNA-seq Library Prep Kit for Illumina (NR605-0, Vazyme), followed by sequencing on the Illumina NovaSeq X Plus platform with the 150 paired-end sequencing strategy. Average loading amount per library for sequencing was 80 ng. mRNA enrichment, library construction, sequencing, and data analysis were performed by Shanghai XuRan Biotechnology Co., Ltd. (http://www.xurangene.com). Raw data were handled by Skewer v0.2.2 (https://sourceforge.net/projects/skewer/files/?source=navbar), and data quality was checked using FastQC v0.11.2 (http://www.bioinformatics.babraham.ac.uk/projects/fastqc/). Read length was 2×150 bp. Clean reads were aligned to the human genome (GRCh38) from the ensemble using STAR (https://github.com/alexdobin/STAR), with one mismatch allowed. StringTie (v1.3.1c) was used to generate gene expression data, and differential gene expression was analyzed using DESeq2 (v1.16.1) (https://bioconductor.org/packages/release/bioc/html/DESeq2.html). Thresholds for determining differentially expressed genes (DEGs) were $p < 0.05$ and an absolute fold change ≥ 1. DEGs were chosen for functional and signaling pathway enrichment analyses using TopGO (https://www.bioconductor.org/packages/release/bioc/html/topGO.html) and KEGG databases (https://www.genome.jp/kegg/pathway.html). Significantly enriched pathways were determined at $p < 0.05$.

Tissue Immunofluorescence

Tissue samples were fixed in 4% paraformaldehyde for 24 h, dehydrated using an alcohol gradient, and cleared in xylene. The tissue was then embedded in paraffin and sectioned at 5 μm on slides. The sections were dewaxed in xylene, rehydrated through an alcohol gradient, and subjected to antigen retrieval in citrate buffer using a microwave. The sections were then blocked with serum for 30 min at room temperature (RT, about 20°C −25°C). Sections were incubated with primary antibody overnight at 4°C. After phosphate buffered saline (PBS) washing, cells were incubated with a fluorescent secondary antibody for 1 h in the dark at RT. Finally, the cells were mounted with 4′,6-diamidino-2-phenylindole and examined under a fluorescence microscope.

Hematoxylin-Eosin Staining (H&E) and Immunohistochemistry (IHC)

Tissue sections were deparaffinized, rehydrated, and successively stained with H&E, followed by dehydration, clearing, and mounting. Tissue sections from the same wax block used for H&E staining were used for IHC analysis.

Western Blot (WB) Assay

Pancreatic tumor tissue proteins were extracted by homogenizing fresh tissue in radioimmunoprecipitation assay (RIPA) buffer containing protease and phosphatase inhibitors. A bicinchoninic acid assay kit (WB6501, New Cell & Molecular Biotech Co., Ltd.) was used to determine total protein concentration. Samples were adjusted to a uniform concentration with RIPA buffer, mixed with loading buffer (5×), boiled, and centrifuged. SDS-PAGE was used for protein separation, followed by blotting onto PVDF membranes. After blocking with 5% non-fat milk, the membranes were incubated overnight at 4°C with primary antibodies and then for 1 h at RT with secondary antibodies. Protein bands were quantified using ImageJ software v1.47. The antibodies used for WB were Janus kinase 1 (Jak1; Proteintech, 66466-1-Ig), phospho-Jak1 (Tyr1034/1035; CST, 74129S), STAT3 (Proteintech, 60199-1-Ig), phospho-Stat3 (Tyr705; CST, 9145T), arginase-1 (ARG-1; Proteintech, 66129-1-g), interleukin (IL)-10 (Proteintech, 60269-1-lg), peroxisome proliferator activated receptor gamma (PPARγ; CST, 2435), beta actin monoclonal antibody (Proteintech, 66009-1-Ig), GAPDH monoclonal antibody (Proteintech, 60004-1-Ig), HRP-conjugated goat anti-rabbit IgG (H+L; Proteintech, SA00001-2), and HRP-conjugated goat-anti-mouse IgG (H+L; Proteintech, SA00001-1). Triplicate data are shown in Supplementary Material 1.

Data Sources for Bioinformatics Analysis

The datasets used to analyze the mRNA expression and survival levels of estrogen receptor 1 (ESR1), EGFR, SRC, AKT1, and STAT3 were sourced from Gene Expression Profiling Interactive Analysis (GEPIA, http://gepia.cancer-pku.cn/). Results with no significant differences are shown in Figure S1.

Statistical Analysis

Statistical analyses and graph construction were performed using GraphPad Prism 10. Data are presented as mean ± standard deviation (SD). To examine the notable disparities across multiple groups, we initially performed normality and variance homogeneity assessments. When data followed a normal distribution and showed uniformity in variance, we used one-way analysis of variance. Whensample size (n) was < 5, permutation tests were conducted on the experimental data. Values of $p < 0.05$ were considered statistically significant. Images were captured and analyzed using IVIS imaging software (Living Imaging, PerkinElmer, USA).

Results

MSJZD Suppressed Pancreatic Tumor Growth in vivo

To ascertain whether MSJZD could inhibit tumor growth in vivo, an orthotopic PC cell transplantation model was established in C57/BL6 mice to evaluate its efficacy. Compared with the NS group, both tumor size and weight were significantly diminished after treatment in the MSJZD-L and MSJZD-H groups (Figure 1A and B). On the 21st day post-treatment with MSJZD-L and MSJZD-H, tumor growth signals markedly reduced (Figure 1C and D). IHC analysis demonstrated that a relatively high percentage of Ki-67 positive cells were present in the NS group, indicating that the

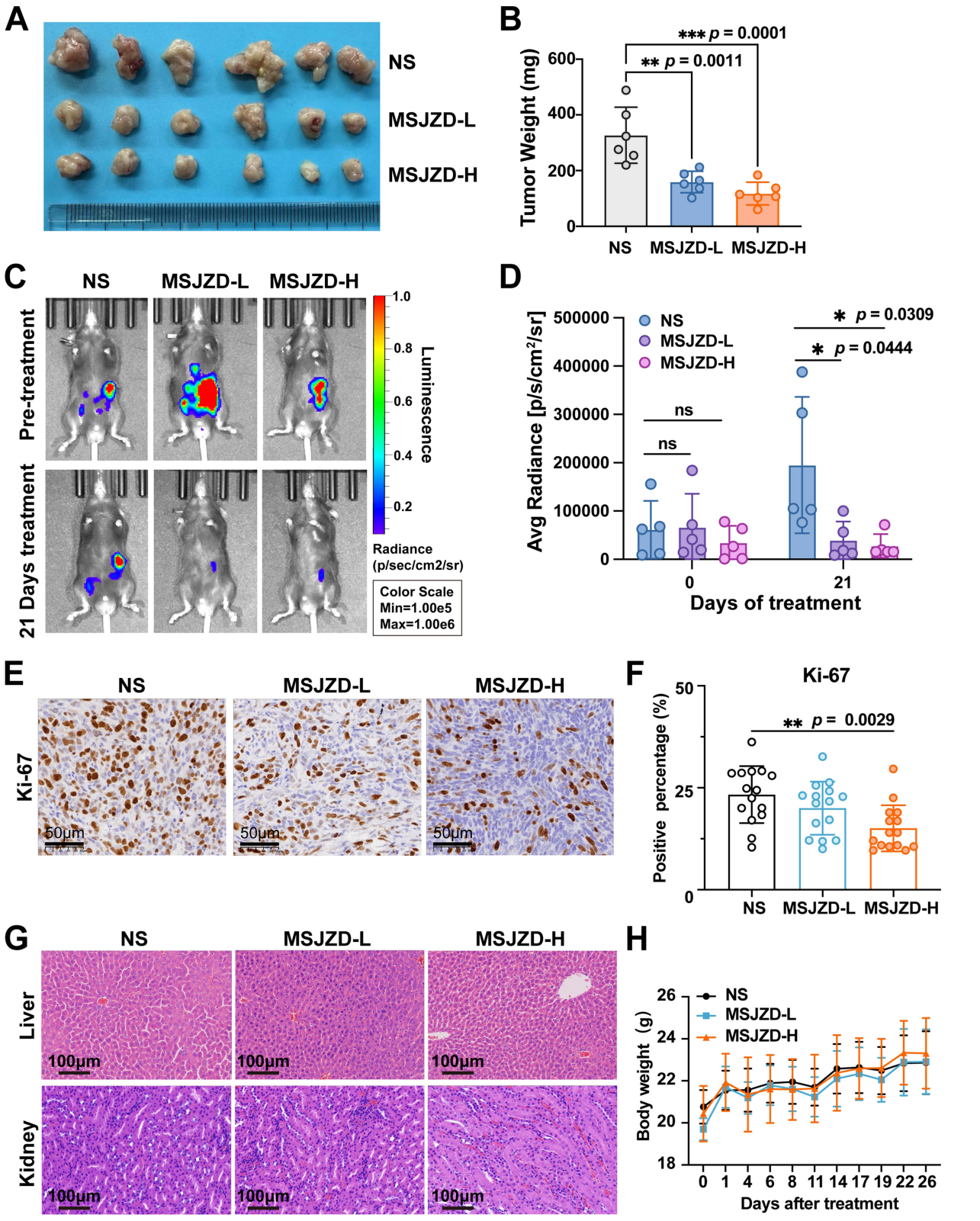

Figure 1 MSJZD suppressed tumors in an orthotopic pancreatic cancer mouse model. (**A**) Tumors of mouse in NS, MSJZD-L and MSJZD-H (n=6/group); (**B**) Tumor weights among three groups over time; (**C**) The average radiance of orthotopic pancreatic cancer mice; (**D**) Statistical plot of the average radiance of orthotopic pancreatic tumors (n=5/group); (**E**) The expression of Ki-67 (IHC, 400×); (**F**) Quantitation of IHC positive percentage of Ki-67 within tumor tissues from 3 Groups (n=5/group), and each dot represent one field of view (FOV) from one sample; (**G**) HE staining of mouse liver and kidney tissues (200×, n=5/group). (**H**) Body weight among three groups (n=6/group). * $p < 0.05$, ** $p < 0.01$, *** $p < 0.001$.

 https://doi.org/10.2147/DDDT.S520390

tumor tissue was actively proliferating. When high-dose MSJZD was administered, the quantity of Ki-67 positive cells decreased notably (Figure 1E and F). Additionally, H&E staining of the liver and kidneys revealed no obvious damage in the MSJZD-L and MSJZD-H groups (Figure 1G), and no abnormal changes in the body weight of the mice were detected (Figure 1H). Collectively, these results suggest that MSJZD exhibits favorable anti-tumor efficacy and safety.

UHPLC-Q-Exactive-MS Analysis of the MSJZD Chemical Constituents

A total of 860 components were identified in MSJZD using UHPLC-Q-Exactive-MS analysis. A base peak chromatogram was obtained by continuously plotting the intensity of the strongest ions in the mass spectrum at each time point (Figure 2A and B). Components, such as endogenous metabolites, intermediates, and synthetic products, were filtered out, and the remaining components were uploaded to the Swiss ADME database (http://www.swissadme.ch/). According to Lipinski's rule for drug-likeness, 206 active ingredients were preliminarily screened (Table S4).

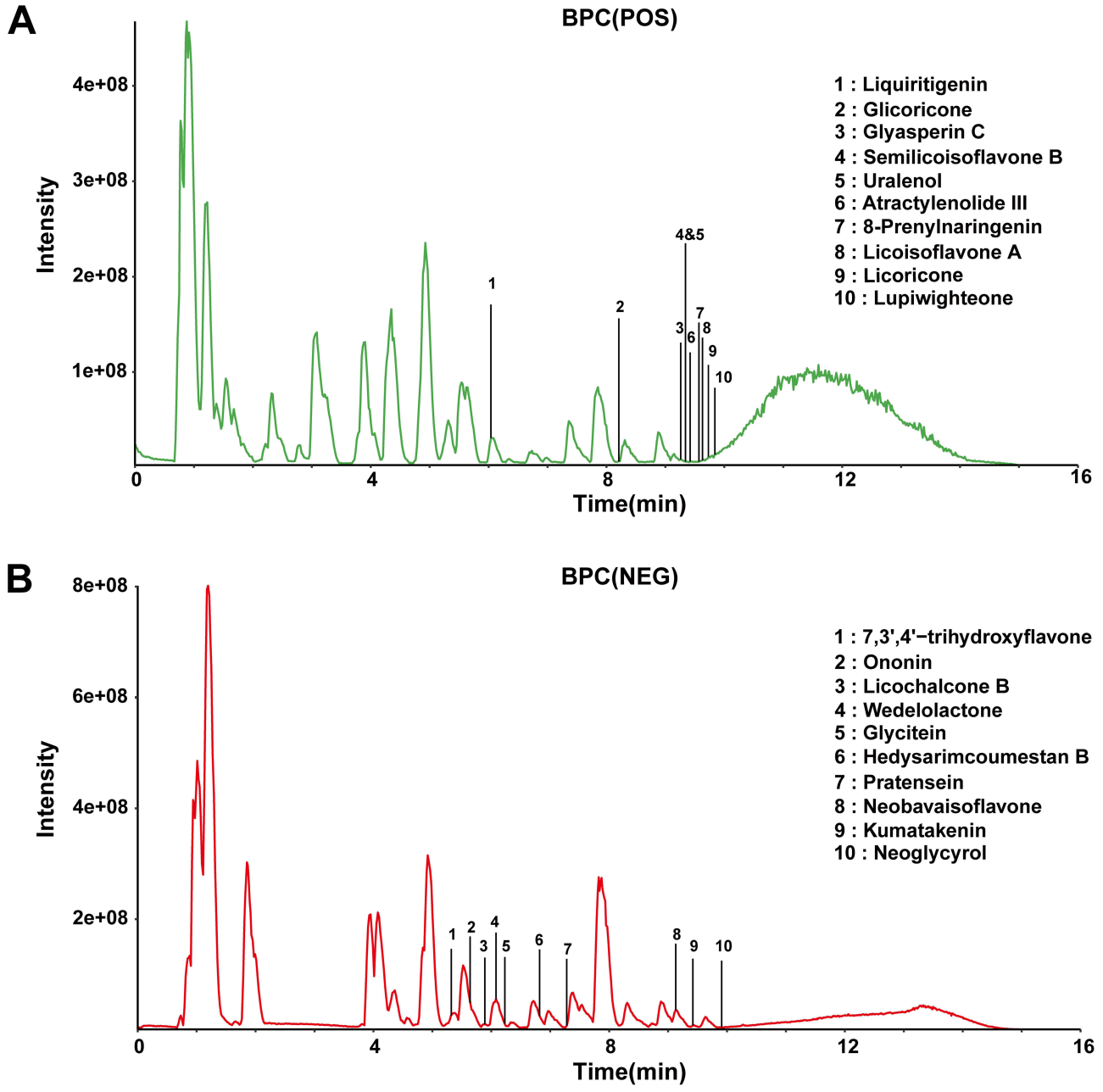

Figure 2 BPC of MSJZD Analyzed by UHPLC-QE-MS and Identified Active Compounds. (**A**) The positive-ion mode; (**B**) The negative-ion mode.

https://doi.org/10.2147/DDDT.S520390

Network Pharmacology Analysis Result

From TCGA, TTD, GeneCards, and OMIM databases, 3915 PC related disease targets were obtained after deduplication (Figure 3A). Using SwissTargetPrediction and TargetNet databases, 1001 targets related to MSJZD components were identified and intersected with PC disease targets, yielding 482 targets (Figure 3B). These 482 targets were input into the

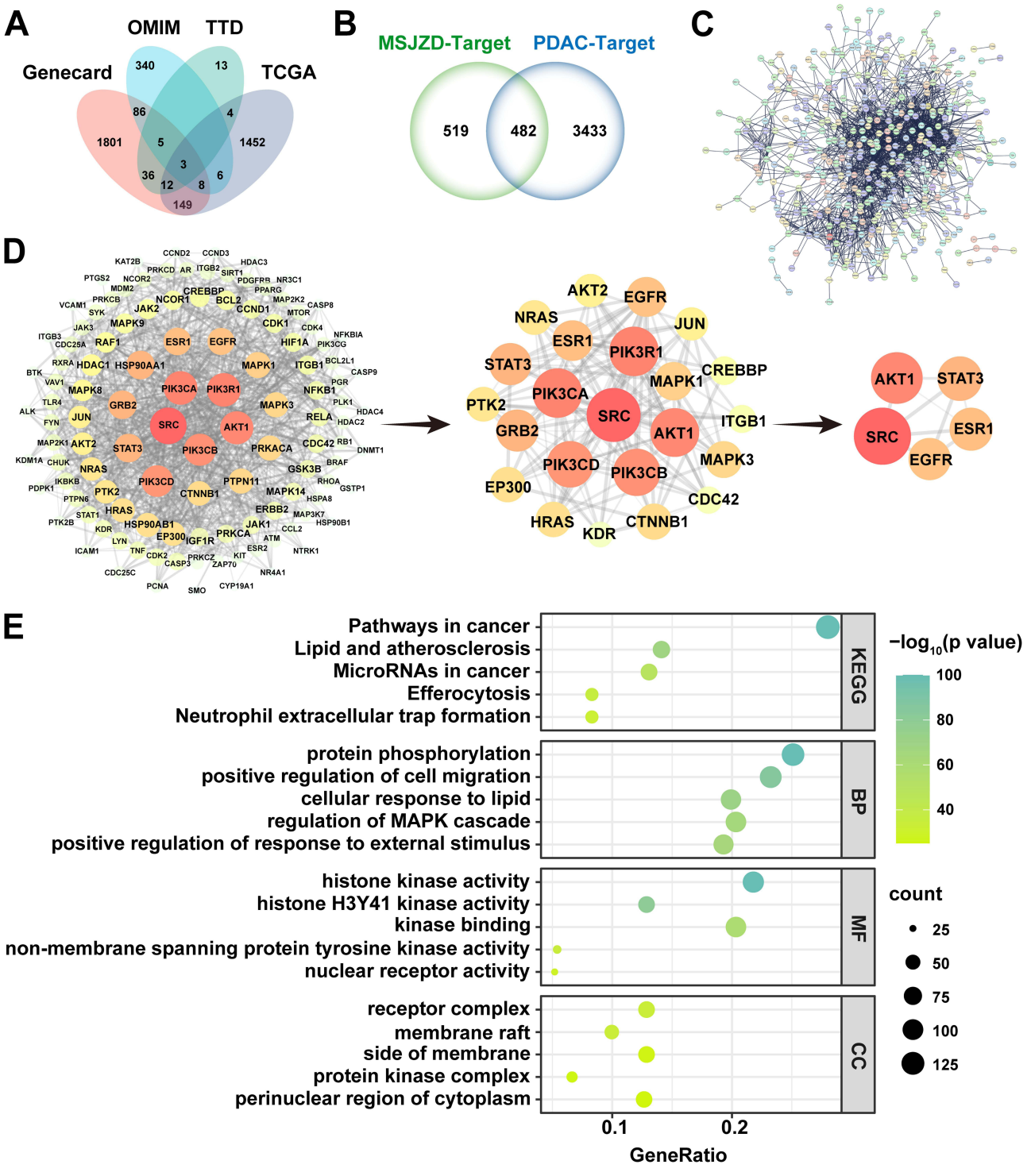

Figure 3 Network pharmacology analysis of MSJZD and PC. (**A**) The Venn diagram of PC targets; (**B**) The Venn diagram of active ingredient targets of MSJZD and PC targets; (**C**) PPI network of targets of MSJZD treatment in PC by STRING database; (**D**) PPI network of targets of MSJZD treatment in PC visualized by Cytoscape 3.7.0 and screened by CytoNCA; (**E**) KEGG pathway enrichment analysis and GO enrichment analysis of 466 overlapping targets.

STRING database to build a PPI network, which was visualized using Cytoscape 3.7.0, resulting in a network with 413 nodes and 1985 edges (Figure 3C). Analysis of centrality measures (DC, BC, CC, EC, IC, LAC, and NC) using the CytoNCA tool and three rounds of screening identified five core target genes: *SRC, ESR1, EGFR, AKT1*, and *STAT3* (Figure 3D). Using the Metascape platform, 482 overlapping targets were used to conduct GO and KEGG enrichment analyses to explore the associations between these targets and diseases. Results of KEGG, BP, CC, and MF analyses were generated based on $-\log_{10}(P)$ values (Figure 3E). MSJZD exerted its therapeutic efficacy via microRNAs in cancer (hsa05206), the efferocytosis pathway (hsa04148), and neutrophil extracellular trap formation (hsa04613). MSJZD achieves its therapeutic objectives by orchestrating an array of biological processes. These included promotion of protein phosphorylation (GO:0006468), cellular response to lipids (GO:0071396), and regulation of the MAPK cascade (GO:0043408).

Gene Expression and Survival Analysis

The expression of five core genes (*SRC, ESR1, EGFR, AKT1*, and *STAT3*) in PC and normal tissues was analyzed using the GEPIA database. The results showed that *SRC, AKT1*, and *STAT3* expression levels were higher in PC tissues (Figure 4A). Survival analysis showed that high *EGFR* expression was associated with shorter overall survival in PC patients (cutoff = 0.5, p = 0.029, Figure 4B).

Molecular Docking Simulations

According to the results of the GEPIA database analysis, EGFR, SRC, AKT1, and STAT3 were selected for subsequent molecular docking. The binding energies between each and all relevant active ingredients and positive drugs were calculated (Tables S2 and S3). The binding energies between the active ingredients and the STAT3 protein were all below the threshold. Subsequently, the active ingredients, uralenol, licoisoflavone A, and wedelolactone, with the highest binding energies to SRC, EGFR, and AKT1 were selected for visualization (Figure 5A–C).

MSJZD Suppressed JAK-STAT Pathway Activity in Tumors in vivo

RNA-seq was performed on tumor tissues from the NS and MSJZD-H groups. Compared with the NS group, 511 genes were downregulated and 691 were upregulated in the MSJZD-H group (Figure 6A). KEGG enrichment analysis of the 511 downregulated genes showed that they mainly participated in the JAK-STAT, PPAR, tumor necrosis factor (TNF), and IL-17 signaling pathways (Figure 6B). A cluster heatmap revealed that multiple upstream stimulatory and receptor genes in the JAK-STAT pathway were downregulated in the MSJZD-H group (Figure 6C). WB detected the expression of key JAK-STAT pathway proteins in tumor tissues, and the results showed down-regulation of JAK1, total STAT3, and its phosphorylation (Figure 6D and E). These results suggest that MSJZD may exert its anti-PC effects by inhibiting the JAK1-STAT3 pathway.

MSJZD Treatment Reduced M2 Macrophage Infiltration

Within the PC microenvironment, tumor-associated macrophages (TAMs) are categorized into two distinct polarization states: classically activated "M1" macrophages and alternatively activated "M2" macrophages.[25] M1-like TAMs are considered anti-tumorigenic and express IL-12, TNF, and inducible nitric oxide synthase. M2-like TAMs have protumorigenic and immunosuppressive properties. They secrete ARG1, PPARγ, and immunosuppressive factors IL-10 and transforming growth factor beta (TGF-β).[26–30]

To verify whether MSJZD can improve the immunosuppressive PC microenvironment by inhibiting macrophages, IHC was used to detect macrophage ($F4/80^+$) expression in tumor tissues. The results showed no difference in overall macrophage infiltration after MSJZD treatment (Figure 7A and B). Multiplex immunofluorescence co-localization analysis revealed a significant increase in M1 macrophage ($F4/80^+CD86^+$) infiltration (Figure 7C and D) in the MSJZD-L and MSJZD-H groups. In contrast, M2 macrophage ($F4/80^+CD206^+$) infiltration was significantly decreased in the MSJZD-H group compared to that in the MSJZD-L group (Figure 7E and F). These results suggested that MSJZD inhibited M2 macrophage polarization in the PC microenvironment in a dose-dependent manner.

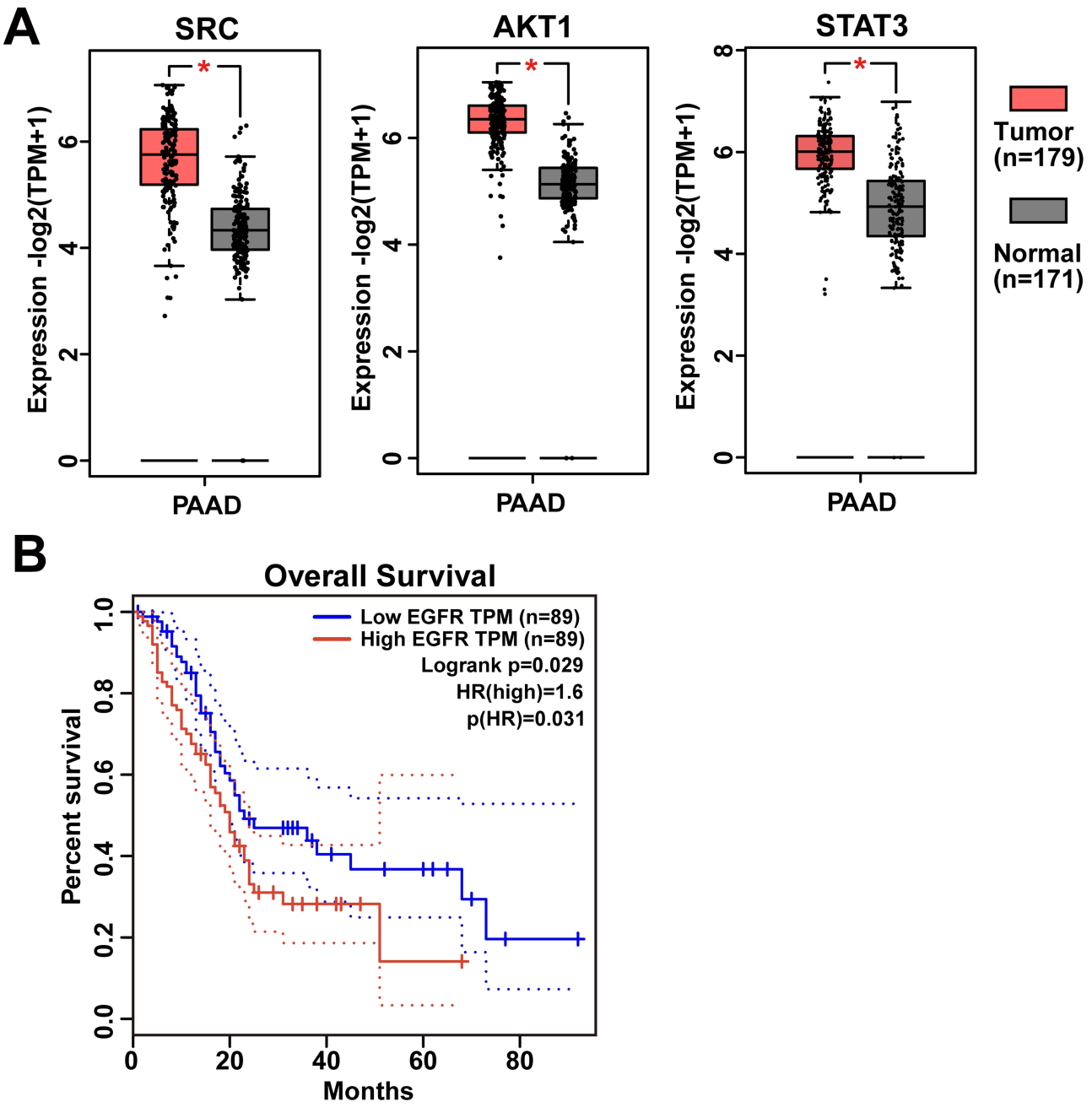

Figure 4 Analyses of target genes expression and survival based on the GEPIA Database. (**A**) Core gene expression between tumor and normal tissues; (**B**) Survival analyses of EGFR expression in PC. * $p < 0.05$.

RNA-seq profiling revealed that among the DEGs between the NS and MSJZD-H groups, the Log_2 fold change in IL-10 and ARG1 was markedly downregulated after MSJZD treatment (Figure 8A and B). Meanwhile, WB and IHC results corroborated a substantial decrease in the expression levels of M2-associated proteins (ARG1, IL-10, IL-6, and PPARγ) after MSJZD treatment (Figure 8C–F). These findings are aligned with the immunofluorescence results.

MSJZD Treatment Increased $CD8^+$ T-Cell Infiltration

ARG1 is secreted by M2 macrophages and consumes L-arginine, which is crucial for T-cell function.[27] To clarify whether the reduction in ARG1 after MSJZD treatment affected T cell survival, immunofluorescence was used to detect

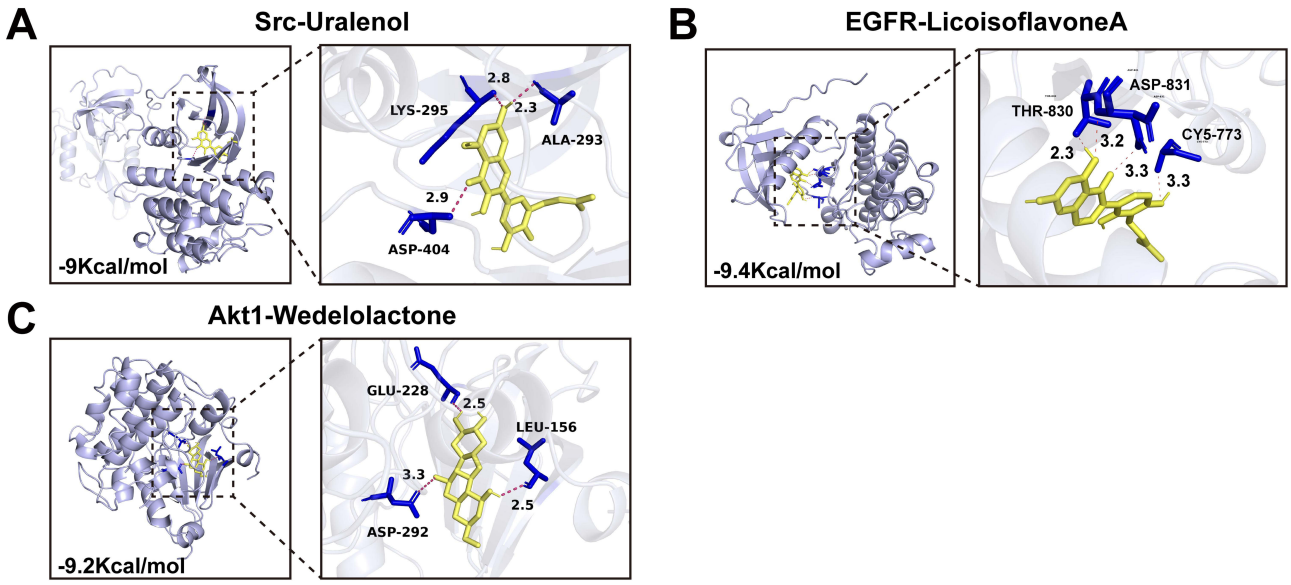

Figure 5 Molecular docking (**A**) Docking visualization of Src and Uralenol; (**B**) Docking visualization of EGFR and Licoisoflavone A; (**C**) Docking visualization of the Akt1 and Wedelolactone.

the infiltration level of $CD8^+$ T cells. The results showed a significant increase in $CD8^+$ T-cell infiltration after MSJZD treatment (Figure 9A and B).

Discussion

The present study demonstrated that MSJZD significantly suppressed tumors in an orthotopic PC mouse model without evident toxicity to the liver and kidneys. *Rhodiola rosea* was recorded in the Tibetan medical classic *Four Medical Tantras* and has been used to treat diseases such as pneumonia and nerve paralysis since the 7th century A.D. Salidroside, the signature active ingredient derived from the *Rhodiola rosea*, exhibits anti-fatigue, neuroprotective, and anti-tumor effects and can inhibit the inflammatory response in acute pancreatitis,[31] suppress PC by improving the hypoxic microenvironment,[32] regulate Tregs cells, and affect the immune microenvironment.[33] The medicinal use of *Dioscorea polystachya* dates back to Shennong's Materia Medica in the Eastern Han Dynasty. It contains a large number of bioactive compounds, such as phenols, flavonoids, saponins, anthocyanins, carotenoids, allantoin, and water-soluble polysaccharides.[34,35] Modern research has confirmed that *Dioscorea polystachya* has cardioprotective, immunoregulatory, anti-tumor, antibacterial, anti-inflammatory, and anti-diabetic effects.[36,37] Combined with the results of this study, it shows that *Rhodiola rosea* and *Dioscorea polystachya* work together with Sijunzi Decoction to exert anti-tumor effects, suggesting the promising clinical therapeutic potential of MSJZD.

Network pharmacology identified SRC, EGFR, AKT1, and STAT3 as key MSJZD targets in PC, with their crosstalk forming a complex regulatory network. The proto-oncogene tyrosine-protein kinase Src regulates tumor cell survival, proliferation, cell adhesion, migration, invasion, and angiogenesis.[38–45] Constitutive activation of Src has been observed in PC,[38] which increases resistance to gemcitabine and promotes the progression of pancreatic ductal adenocarcinoma (PDAC).[46] Src regulates PI3K signaling by directly phosphorylating the p85 subunit of PI3K[47] and inhibiting the PI3K negative regulatory phosphatase and tensin homolog.[48] This leads to downstream phosphorylation of AKT, thereby enhancing the growth and survival of PC cells.[49] Src and STAT3 signaling enhances the transcription of angiogenesis-related genes (such as IL-8 and vascular endothelial growth factor) in human PC cells,[50–52] with STAT3-mediated signaling serving as a key contributor to chemoresistance in PDAC.[53–56] Inhibition of Src activity reduces STAT3 phosphorylation and tumorigenicity.[50] The reciprocal signaling between Src and EGFR drives a more aggressive cancer phenotype by enhancing tumor cell proliferation, invasion, and metastasis[57,58] Regarding the compensatory activation induced by single-target inhibitors, combination therapy has demonstrated stronger anti-tumor activity in preclinical

https://doi.org/10.2147/DDDT.S520390

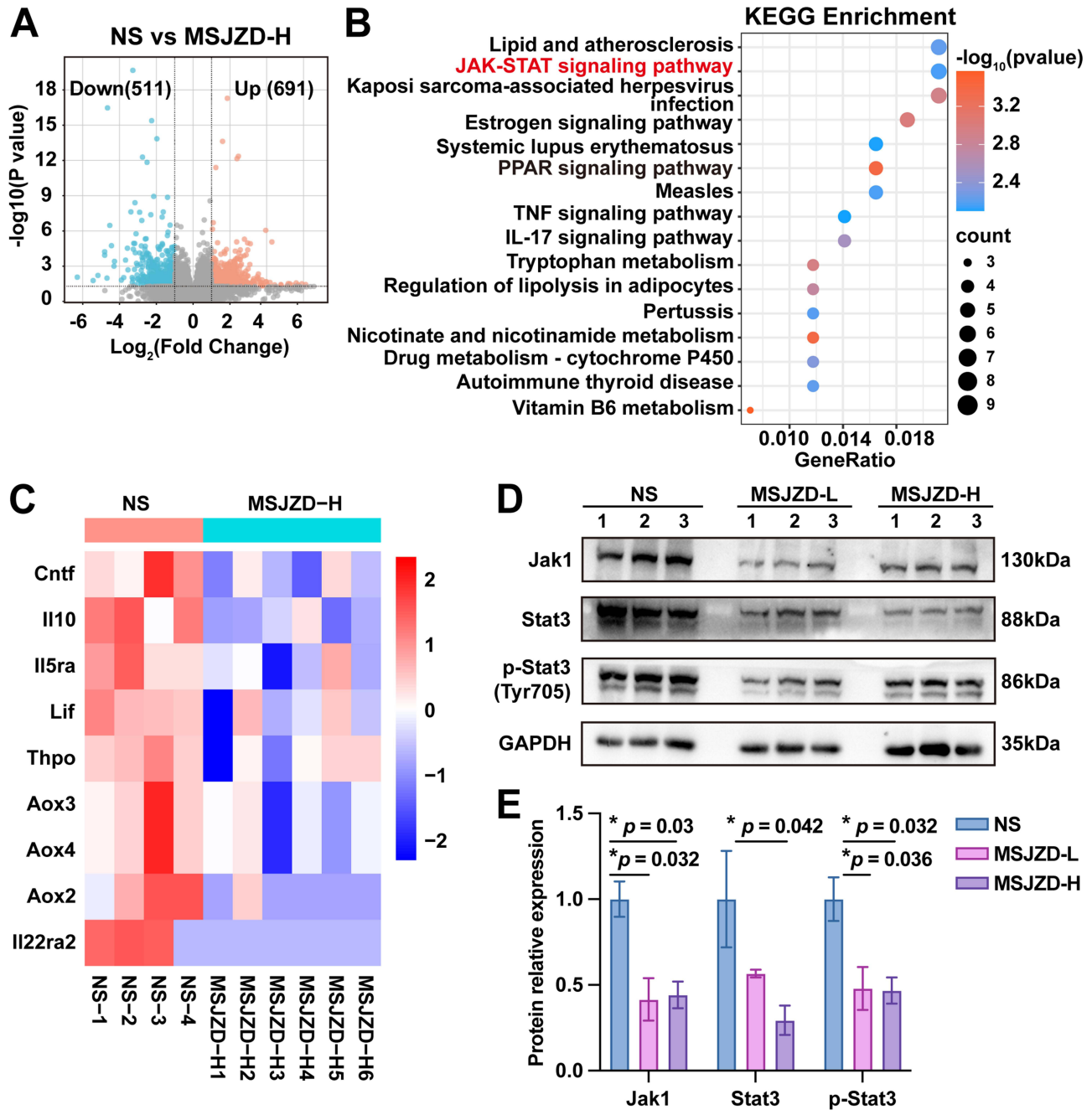

Figure 6 RNA-seq data analysis and experimental validation of tumors after MSJZD treatment. (**A**) Volcano-plot of DGEs (p. adj < 0.05, $Log_2|FC| \geq 1$); (**B**) Enrichment analysis of pathways related to down-regulated genes; (**C**) Clustering map of downregulated genes in the JAK-STAT pathway; (**D**) WB validation of the downregulation of key proteins in the JAK-STAT pathway; (**E**) Statistical analysis chart of WB. * $p < 0.05$. **Abbreviation**: JAK-STAT, Janus kinase-signal transducer and activator of transcription.

models. For instance, triple therapy with dasatinib (an Src inhibitor), erlotinib (an EGFR inhibitor), and gemcitabine synergistically inhibits cancer cell proliferation and xenograft tumor growth,[56] overcomes constitutive STAT3 activation, shows good tolerability, and exhibits preliminary efficacy in advanced PC.[59]

The results showed that the JAK-STAT pathway was significantly downregulated after MSJZD treatment. Triggered by specific cytokine-receptor interactions leading to receptor dimerization or multimerization, the JAK-STAT pathway activates JAK, phosphorylates STAT, initiates transcriptional events,[60,61] and regulates immune cell (B and T lymphocyte, natural killer cell, macrophage, and dendritic cell) development, activation, and function.[61] The JAK-

 https://doi.org/10.2147/DDDT.S520390

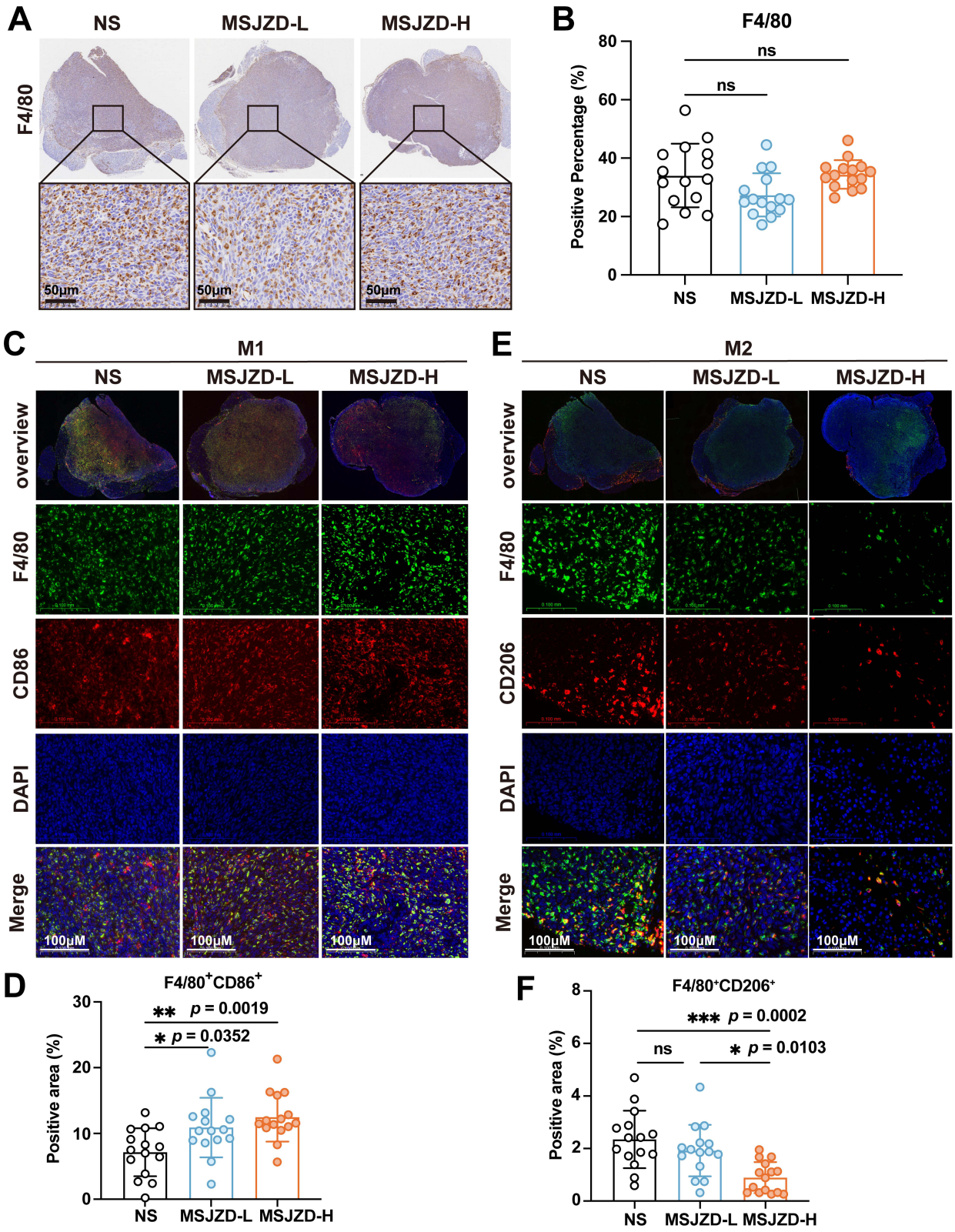

Figure 7 Polarization of Macrophages in NS, MSJZD-L and MSJZD-H tumor tissues. (**A**) IHC detection of F4/80 expression in NS, MSJZD-L and MSJZD-H groups; (**B**) Statistical chart of F4/80 expression; (**C** and **D**) IF detection and statistical analysis of the expression of F4/80+CD86+ macrophages in NS, MSJZD-L and MSJZD-H groups; (**E** and **F**) IF detection and statistical analysis of the expression of F4/80+CD206+ macrophages in NS, MSJZD-L and MSJZD-H groups; n=5/group. Each dot: one FOV from one sample. * $p < 0.05$, ** $p < 0.01$, *** $p < 0.001$.

Abbreviations: M1, M1-like macrophages; M2, M2-like macrophages.

https://doi.org/10.2147/DDDT.S520390

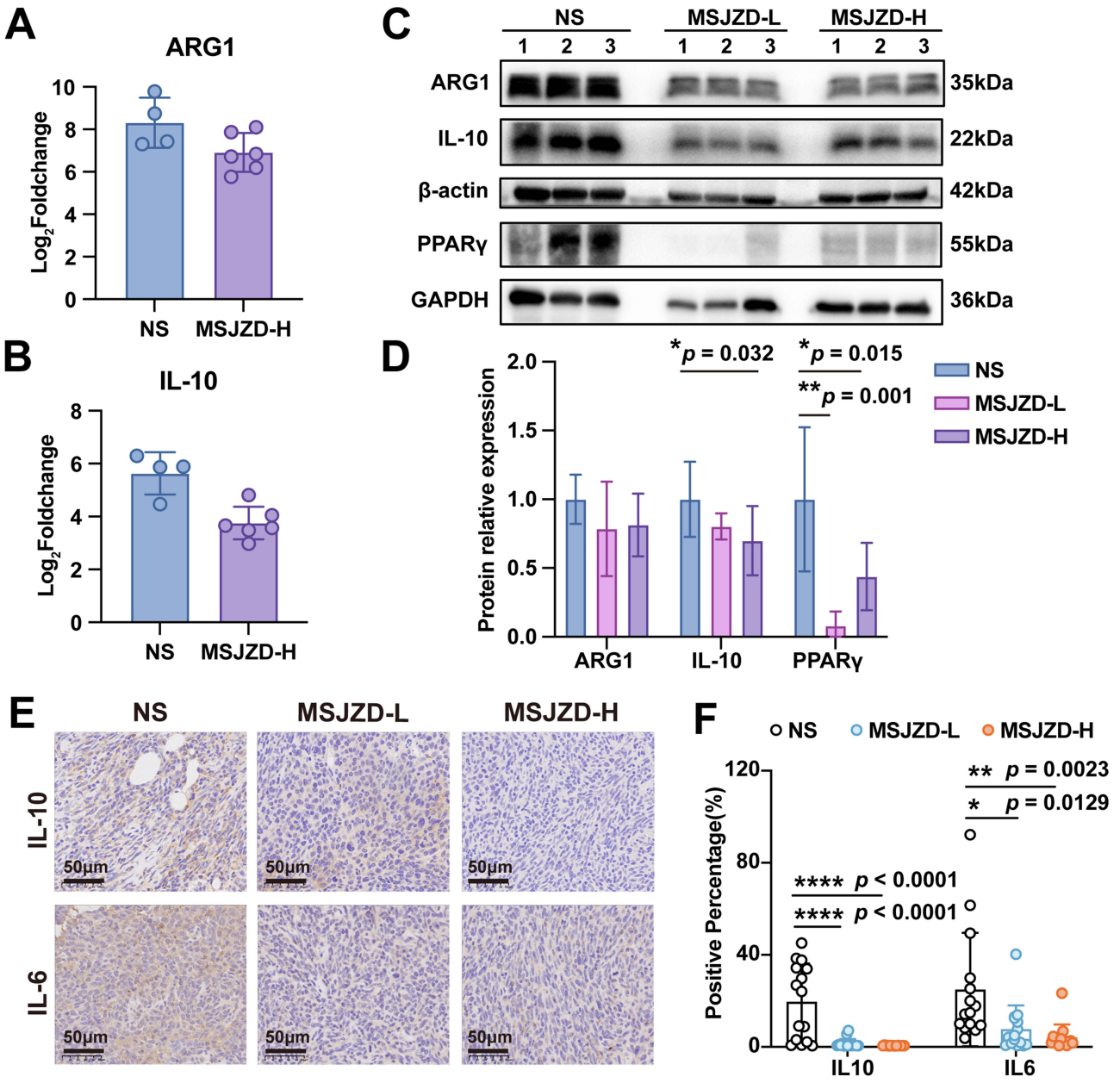

Figure 8 Expression of M2 macrophage-related proteins reduced after MSJZD treatment. (**A** and **B**) Expression levels of Log_2foldchange of IL-10 and ARG1 in NS and MSJZD-H group (**C** and **D**) Expression levels and statistical analysis of M2 macrophages-related protein in NS, MSJZD-L and MSJZD-H group (n=3 per group); (**E**) IHC detection of IL-10, IL-6 expression in NS, MSJZD-L and MSJZD-H groups; (**F**) Statistical chart of IL-10, IL-6 expression. n=5/group. Each dot: one FOV from one sample. * $p < 0.05$, ** $p < 0.01$, **** $p < 0.0001$.

STAT pathway coordinates immune responses, inflammation, homeostasis, tumor surveillance, and abnormal cell clearance by regulating immune cell differentiation, activation, proliferation, and immune mediator production.[61–65] STAT3 regulates the immune response of macrophages and is a key signal for their polarization to the M2 phenotype.[66–68] In a variety of solid tumors, IL-10 and IL-6 secreted by TAMs can activate STAT3,[69,70] which further promotes IL-10 and IL-6 transcription and expression,[71,72] thus forming a positive-feedback loop to promote tumor progression.

KEGG enrichment analysis revealed the significant downregulation of multiple signaling pathways following MSJZD treatment, including the TNF, IL-17, and PPAR signaling pathways, indicating broad effects on inflammation and lipid metabolism. The PPAR signaling pathway regulates lipid and glucose metabolism, inflammation, and cell differentiation. PPARγ acts as a master transcriptional regulator, governing downstream genes involved in mitochondrial function and

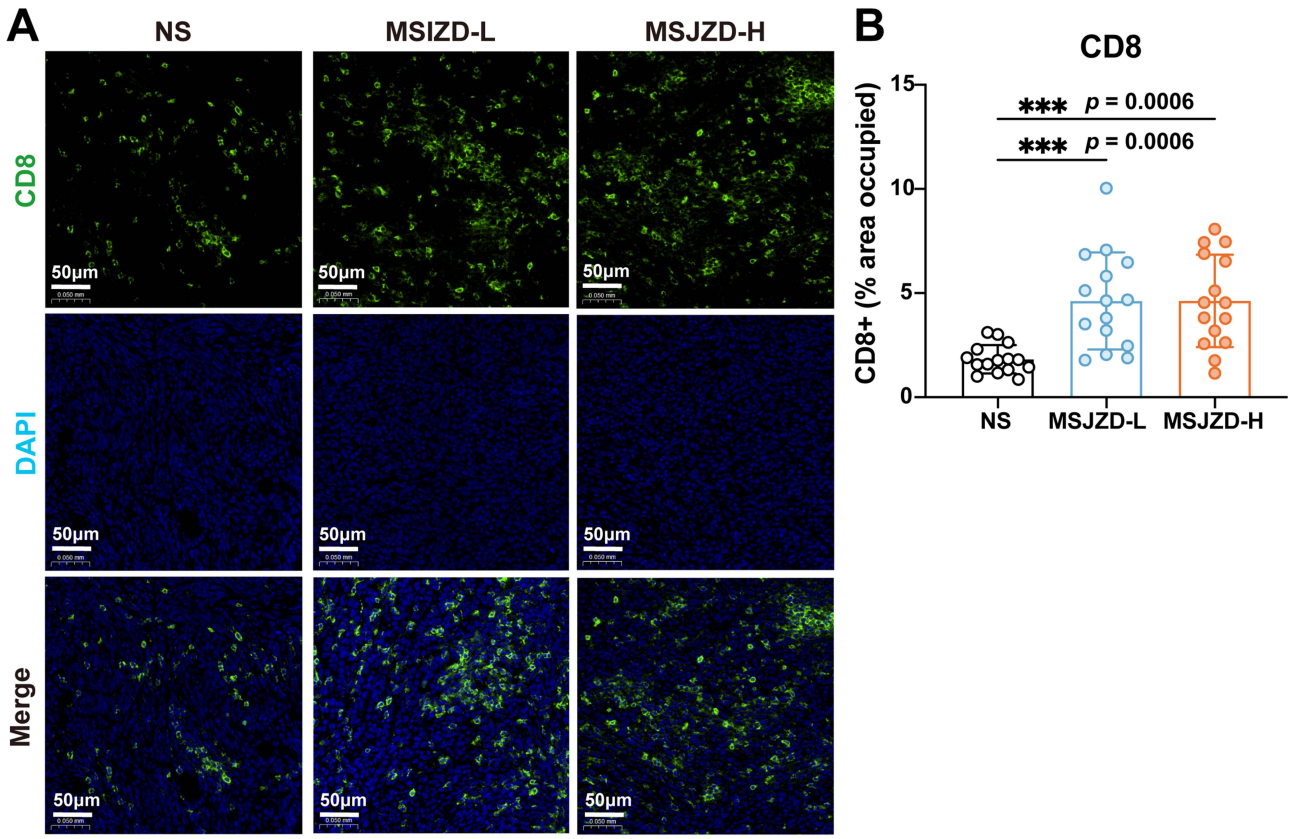

Figure 9 $CD8^+$ T cell infiltration increased after MSJZD treatment. (**A**) $CD8^+$ T cell infiltration in NS, MSJZD-L and MSJZD-H tumor tissues. (**B**) statistical analysis of the expression of CD8+ T cell in NS, MSJZD-L and MSJZD-H groups. n=5/group. Each dot: one FOV from one sample. *** $p < 0.001$.

redox balance.[73–75] Specifically, PPARγ activation has been shown to promote PC cell proliferation both in vitro and in vivo, while upregulating superoxide dismutase 2 to mitigate mitochondrial reactive oxygen species production, stabilize mitochondrial membrane potential, and suppress apoptosis.[76] Targeting PPARγ may thus represent a strategy to identify MSJZD components that modulate lipid metabolism and exert anti-tumor effects.

This study demonstrated that MSJZD exerts anti-tumor effects through multiple targets and pathways, showing great therapeutic potential. Further evaluation of the toxicity and lethal doses of the individual herbs and the compound formula in MSZJD is needed to improve safety assessments.

The current study focused on characterizing the standalone anti-PC effects of MSJZD, rather than direct efficacy comparisons with existing therapies, thereby isolating and validating its unique pharmacological profile without introducing comparative confounders. Given that MSJZD exerted effects in anti-tumor activity and immunosuppression modulation, future clinical trials exploring combination strategies using chemotherapeutic agents, molecularly targeted drugs, and immune checkpoint inhibitors are warranted. Although this study predicted active ingredient-target binding strength via molecular docking with binding energy calculations, future research should overcome equipment limitations to validate active ingredient-target affinity and drug-receptor binding kinetics using surface plasmon resonance technology. The PC tumor microenvironment is complex, highly heterogeneous, and contains abundant immune and stromal cells. It is essential to further elucidate the molecular mechanisms underlying the inhibition of M2 macrophage polarization-mediated immunosuppressive microenvironments and to systematically evaluate the immune response activity of $CD8^+$ T cells through in vitro and in vivo functional assays. Single-cell RNA sequencing and CyTOF mass cytometry will be employed to profile immune subset dynamics to comprehensively reveal changes in the PC microenvironment immune landscape and the key immunoregulatory mechanisms following MSJZD intervention. Owing to limited sample availability, Western blotting results (n=3/group) had severely limited statistical power, which was

https://doi.org/10.2147/DDDT.S520390

mitigated by robustness-correcting permutation tests. Replication in larger cohorts is required to validate the generalizability of this effect.

Conclusions

This study demonstrated the effectiveness and safety of MSJZD. It exerts anti-tumor effects by inhibiting the JAK1-STAT3 pathway, improving the immunosuppressive microenvironment by reducing M2 macrophage infiltration and IL-10 and IL-6 expression, and increasing $CD8^+$ T-cell infiltration. This study reveals the therapeutic potential of MSJZD and offers a reference for further research.

Data Sharing Statement

Data will be available on request.

Acknowledgments

The authors express their sincere gratitude to the researchers and staff associated with the aforementioned software and databases.

Funding

This study received financial support from the National Natural Science Foundation of China. [grant number 81930115 and 82174155].

Disclosure

The authors make a declaration that they do not have any conflicts of interest regarding this piece of work.

References

1. Siegel RL, Kratzer TB, Giaquinto AN, Sung H, Jemal A. Cancer statistics, 2025. *CA Cancer J Clin*. 2025;75(1):10–45. doi:10.3322/caac.21871
2. Park W, Chawla A, O'Reilly EM. Pancreatic Cancer: a Review. *JAMA*. 2021;326(9):851–862. doi:10.1001/jama.2021.13027
3. Gu A, Li J, Li M-Y, Liu Y. Patient-derived xenograft model in cancer: establishment and applications. *MedComm*. 2025;6(2):e70059. doi:10.1002/mco2.70059
4. Gu A, Li J, Qiu S, et al. Pancreatic cancer environment: from patient-derived models to single-cell omics. *Mol Omics*. 2024;20(4):220–233. doi:10.1039/d3mo00250k
5. Cong B. Perspectives in Food & Medicine Homology. *Food Med Homol*. 2024;1(1):9420018. doi:10.26599/FMH.2024.9420018
6. Sun-Waterhouse D-X, Chen X-Y, Liu Z-H, I.N. Waterhouse G, Kang W-Y. Transformation from traditional medicine-food homology to modern food-medicine homology. *Food Med Homol*. 2024;1(1):9420014. doi:10.26599/FMH.2024.9420014
7. Li M-Y, Gu A, Li J, et al. Exploring food and medicine homology: potential implications for cancer treatment innovations. *Acta Materia Medica*. 2025;4(2). doi:10.15212/amm-2025-0003
8. Wang X, Pan S, Chen L, et al. Sijunzi decoction enhances sensitivity of colon cancer cells to NK cell destruction by modulating P53 expression. *J Ethnopharmacol*. 2024;329:118115. doi:10.1016/j.jep.2024.118115
9. Wong H-L, W-s S, W-t S, Gao S, Leung P-C, Ko C-H. Application of Chinese herbal medicines to revitalize adult stem cells for tissue regeneration. *Chin J Integr Med*. 2012;18(12):903–908. doi:10.1007/s11655-012-1293-3
10. Wu B, Z-r X. Progress in research on applying Sijunzi Decoction in treating digestive malignant tumor. *Chin J Integr Med*. 2007;13(2):156–159.
11. Zhu Y, Ma R, Cheng W, et al. Sijunzi decoction ameliorates gastric precancerous lesions via regulating oxidative phosphorylation based on proteomics and metabolomics. *J Ethnopharmacol*. 2024;318(Pt A):116925. doi:10.1016/j.jep.2023.116925
12. Shang L, Wang Y, Li J, et al. Mechanism of Sijunzi Decoction in the treatment of colorectal cancer based on network pharmacology and experimental validation. *J Ethnopharmacol*. 2023;302(Pt A):115876. doi:10.1016/j.jep.2022.115876
13. Pu W-L, Zhang M-Y, Bai R-Y, et al. Anti-inflammatory effects of Rhodiola rosea L.: a review. *Biomed Pharmacother*. 2020;121:109552. doi:10.1016/j.biopha.2019.109552
14. Xiong Y-X, Li N, Han -M-M, et al. Rhodiola rosea polysaccharides-based nanoparticles loaded with DOX boosts chemo-immunotherapy for triple-negative breast cancer by re-educating Tumor-associated macrophages. *Int J Biol Macromol*. 2023;239:124110. doi:10.1016/j.ijbiomac.2023.124110
15. Cai Z, Li W, Wang H, et al. Antitumor effects of a purified polysaccharide from Rhodiola rosea and its action mechanism. *Carbohydr Polym*. 2012;90(1):296–300. doi:10.1016/j.carbpol.2012.05.039
16. Rong L, Li Z, Leng X, et al. Salidroside induces apoptosis and protective autophagy in human gastric cancer AGS cells through the PI3K/Akt/mTOR pathway. *Biomed Pharmacother*. 2020;122:109726. doi:10.1016/j.biopha.2019.109726
17. Nagai T, Suzuki N, Kai N, Tanoue Y. Functional properties of autolysate and enzymatic hydrolysates from yam tsukuneimo (Dioscorea opposita Thunb.) tuber mucilage tororo: antioxidative activity and antihypertensive activity. *J Food Sci Technol*. 2014;51(12):3838–3845. doi:10.1007/s13197-012-0910-x

18. Hao L-X, Zhao X-H. Immunomodulatory potentials of the water-soluble yam (Dioscorea opposita Thunb) polysaccharides for the normal and cyclophosphamide-suppressed mice. *Food Agric Immunol*. 2016;27(5):667–677. doi:10.1080/09540105.2016.1148666
19. Liu X, Chen X, Xie L, Xie J, Shen M. Sulfated Chinese yam polysaccharide enhances the immunomodulatory activity of RAW 264.7 cells via the TLR4-MAPK/NF-κB signaling pathway. *Food Funct*. 2022;13(3):1316–1326. doi:10.1039/d1fo03630k
20. Huang R, Shen M, Yu Y, Liu X, Xie J. Physicochemical characterization and immunomodulatory activity of sulfated Chinese yam polysaccharide. *Int J Biol Macromol*. 2020;165(Pt A):635–644. doi:10.1016/j.ijbiomac.2020.09.213
21. Choi EM, Koo SJ, Hwang J-K. Immune cell stimulating activity of mucopolysaccharide isolated from yam (Dioscorea batatas). *J Ethnopharmacol*. 2004;91(1):1–6.
22. Ma F, Wang R, Zhang Y, et al. Polysaccharides from Dioscorea opposita Thunb.: isolation, structural characterization, and anti-inflammatory and anti-tumor effects against hepatocellular carcinoma. *Chem Biol Technol Agri*. 2023;10(1):43. doi:10.1186/s40538-023-00421-8
23. Xu SY, Bian RL, Chen X. *Experimental Methodology of Pharmacology*. Beijing: People's Medical Publishing House; 2002.
24. Chu Z-Y, Zi X-J. Network toxicology and molecular docking for the toxicity analysis of food contaminants: a case of Aflatoxin B1. *Food Chem Toxicol*. 2024;188:114687. doi:10.1016/j.fct.2024.114687
25. Guillot A, Tacke F. Liver macrophages: old dogmas and new insights. *Hepatol Commun*. 2019;3(6):730–743. doi:10.1002/hep4.1356
26. Falcomatà C, Bärthel S, Schneider G, Rad R, Schmidt-Supprian M, Saur D. Context-specific determinants of the immunosuppressive tumor microenvironment in pancreatic cancer. *Cancer Discov*. 2023;13(2):278–297. doi:10.1158/2159-8290.CD-22-0876
27. Geiger R, Rieckmann JC, Wolf T, et al. L-arginine modulates T cell metabolism and enhances survival and anti-tumor activity. *Cell*. 2016;167(3). doi:10.1016/j.cell.2016.09.031
28. Oh SA, Li MO. TGF-β: guardian of T cell function. *J Immunol*. 2013;191(8):3973–3979. doi:10.4049/jimmunol.1301843
29. Propper DJ, Balkwill FR. Harnessing cytokines and chemokines for cancer therapy. *Nat Rev Clin Oncol*. 2022;19(4):237–253. doi:10.1038/s41571-021-00588-9
30. Batlle E, Massagué J. Transforming Growth Factor-β Signaling in Immunity and Cancer. *Immunity*. 2019;50(4):924–940. doi:10.1016/j.immuni.2019.03.024
31. Wang X, Qian J, Meng Y, et al. Salidroside alleviates severe acute pancreatitis-triggered pancreatic injury and inflammation by regulating miR-217-5p/YAF2 axis. *Int Immunopharmacol*. 2022;111:109123. doi:10.1016/j.intimp.2022.109123
32. Chen X, Kou Y, Pu Y, Lu Y. Salidroside ameliorated hypoxia-induced tumorigenesis of BxPC-3 cells via downregulating hypoxia-inducible factor (HIF)-1α and LOXL2. *J Cell Biochem*. 2020;121(1):165–173. doi:10.1002/jcb.29000
33. Wen Z, Liu T, Zhang Y, et al. Salidroside regulates tumor microenvironment of non-small cell lung cancer via Hsp70/Stub1/Foxp3 pathway in Tregs. *BMC Cancer*. 2023;23(1):717. doi:10.1186/s12885-023-11036-5
34. Padhan B, Panda D. Potential of neglected and underutilized Yams (Dioscorea spp.) for improving nutritional security and health benefits. *Front Pharmacol*. 2020;11:496. doi:10.3389/fphar.2020.00496
35. Lebot V, Lawac F, Legendre L. The greater yam (Dioscorea alata L.): a review of its phytochemical content and potential for processed products and biofortification. *J Food Composition Anal*. 2023;115:104987. doi:10.1016/j.jfca.2022.104987
36. Adomėnienė A, Venskutonis PR. Dioscorea spp.: comprehensive review of antioxidant properties and their relation to phytochemicals and health benefits. *Molecules*. 2022;27(8). doi:10.3390/molecules27082530
37. Kundu BB, Vanni K, Farheen A, Jha P, Pandey DK, Kumar V. Dioscorea bulbifera L.(Dioscoreaceae): a review of its ethnobotany, pharmacology and conservation needs. *S Afr J Bot*. 2021;140:365–374. doi:10.1016/j.sajb.2020.07.028
38. Morton JP, Karim SA, Graham K, et al. Dasatinib inhibits the development of metastases in a mouse model of pancreatic ductal adenocarcinoma. *Gastroenterology*. 2010;139(1):292–303. doi:10.1053/j.gastro.2010.03.034
39. Frame MC. Src in cancer: deregulation and consequences for cell behaviour. *Biochim Biophys Acta*. 2002;1602(2):114–130.
40. Je DW, YM O, Ji YG, Cho Y, Lee DH. The inhibition of SRC family kinase suppresses pancreatic cancer cell proliferation, migration, and invasion. *Pancreas*. 2014;43(5):768–776. doi:10.1097/MPA.0000000000000103
41. Ischenko I, Guba M, Yezhelyev M, et al. Effect of Src kinase inhibition on metastasis and tumor angiogenesis in human pancreatic cancer. *Angiogenesis*. 2007;10(3):167–182.
42. Thomas SM, Brugge JS. Cellular functions regulated by Src family kinases. *Annu Rev Cell Dev Biol*. 1997;13:513–609.
43. Ishizawar R, Parsons SJ. c-Src and cooperating partners in human cancer. *Cancer Cell*. 2004;6(3):209–214.
44. Yeatman TJ. A renaissance for SRC. *Nat Rev Cancer*. 2004;4(6):470–480.
45. Serrels A, Macpherson IRJ, Evans TRJ, et al. Identification of potential biomarkers for measuring inhibition of Src kinase activity in colon cancer cells following treatment with dasatinib. *Mol Cancer Ther*. 2006;5(12):3014–3022.
46. Duxbury MS, Ito H, Zinner MJ, Ashley SW, Whang EE. Inhibition of SRC tyrosine kinase impairs inherent and acquired gemcitabine resistance in human pancreatic adenocarcinoma cells. *Clin Cancer Res*. 2004;10(7):2307–2318.
47. Cuevas BD, Lu Y, Mao M, et al. Tyrosine phosphorylation of p85 relieves its inhibitory activity on phosphatidylinositol 3-kinase. *J Biol Chem*. 2001;276(29):27455–27461.
48. Lu Y, Yu Q, Liu JH, et al. Src family protein-tyrosine kinases alter the function of PTEN to regulate phosphatidylinositol 3-kinase/AKT cascades. *J Biol Chem*. 2003;278(41):40057–40066.
49. Murthy D, Attri KS, Singh PK. Phosphoinositide 3-kinase signaling pathway in pancreatic ductal adenocarcinoma progression, pathogenesis, and therapeutics. *Front Physiol*. 2018;9:335. doi:10.3389/fphys.2018.00335
50. Trevino JG, Summy JM, Gray MJ, et al. Expression and activity of SRC regulate interleukin-8 expression in pancreatic adenocarcinoma cells: implications for angiogenesis. *Cancer Res*. 2005;65(16):7214–7222.
51. Liu X, Guo X, Li H, Chen J, Qi X. Src/STAT3 signaling pathways are involved in KAI1-induced downregulation of VEGF-C expression in pancreatic cancer. *Mol Med Rep*. 2016;13(6):4774–4778. doi:10.3892/mmr.2016.5093
52. Wei D, Le X, Zheng L, et al. Stat3 activation regulates the expression of vascular endothelial growth factor and human pancreatic cancer angiogenesis and metastasis. *Oncogene*. 2003;22(3):319–329.
53. Wörmann SM, Song L, Ai J, et al. Loss of P53 function activates JAK2-STAT3 signaling to promote pancreatic tumor growth, stroma modification, and gemcitabine resistance in mice and is associated with patient survival. *Gastroenterology*. 2016;151(1). doi:10.1053/j.gastro.2016.03.010

54. Nagaraj NS, Smith JJ, Revetta F, Washington MK, Merchant NB. Targeted inhibition of SRC kinase signaling attenuates pancreatic tumorigenesis. *Mol Cancer Ther*. 2010;9(8):2322–2332. doi:10.1158/1535-7163.MCT-09-1212
55. Zhao X-K, Cheng Y, Liang Cheng M, et al. Focal adhesion kinase regulates fibroblast migration via integrin beta-1 and plays a central role in fibrosis. *Sci Rep*. 2016;6:19276. doi:10.1038/srep19276
56. Nagaraj NS, Washington MK, Merchant NB. Combined blockade of Src kinase and epidermal growth factor receptor with gemcitabine overcomes STAT3-mediated resistance of inhibition of pancreatic tumor growth. *Clin Cancer Res*. 2011;17(3):483–493. doi:10.1158/1078-0432.CCR-10-1670
57. Maa MC, Leu TH, McCarley DJ, Schatzman RC, Parsons SJ. Potentiation of epidermal growth factor receptor-mediated oncogenesis by c-Src: implications for the etiology of multiple human cancers. *Proc Natl Acad Sci U S A*. 1995;92(15):6981–6985.
58. Biscardi JS, Belsches AP, Parsons SJ. Characterization of human epidermal growth factor receptor and c-Src interactions in human breast tumor cells. *Mol, Carcinog*. 1998;21(4):261–272.
59. Cardin DB, Goff LW, Chan E, et al. Dual Src and EGFR inhibition in combination with gemcitabine in advanced pancreatic cancer: Phase I results: a phase I clinical trial. *Invest New Drugs*. 2018;36(3):442–450. doi:10.1007/s10637-017-0519-z
60. Morris R, Kershaw NJ, Babon JJ. The molecular details of cytokine signaling via the JAK/STAT pathway. *Protein Sci*. 2018;27(12):1984–2009. doi:10.1002/pro.3519
61. Philips RL, Wang Y, Cheon H, et al. The JAK-STAT pathway at 30: much learned, much more to do. *Cell*. 2022;185(21):3857–3876. doi:10.1016/j.cell.2022.09.023
62. Hammarén HM, Virtanen AT, Raivola J, Silvennoinen O. The regulation of JAKs in cytokine signaling and its breakdown in disease. *Cytokine*. 2019;118:48–63. doi:10.1016/j.cyto.2018.03.041
63. Haan C, Kreis S, Margue C, Behrmann I. Jaks and cytokine receptors--an intimate relationship. *Biochem Pharmacol*. 2006;72(11):1538–1546.
64. Anand S, Stedham F, Beer P, et al. Effects of the JAK2 mutation on the hematopoietic stem and progenitor compartment in human myeloproliferative neoplasms. *Blood*. 2011;118(1):177–181. doi:10.1182/blood-2010-12-327593
65. Seif F, Khoshmirsafa M, Aazami H, Mohsenzadegan M, Sedighi G, Bahar M. The role of JAK-STAT signaling pathway and its regulators in the fate of T helper cells. *Cell Commun Signal*. 2017;15(1):23. doi:10.1186/s12964-017-0177-y
66. Takeda K, Clausen BE, Kaisho T, et al. Enhanced Th1 activity and development of chronic enterocolitis in mice devoid of Stat3 in macrophages and neutrophils. *Immunity*. 1999;10(1):39–49.
67. Yu H, Kortylewski M, Pardoll D. Crosstalk between cancer and immune cells: role of STAT3 in the tumour microenvironment. *Nat Rev Immunol*. 2007;7(1):41–51.
68. Petty AJ, Owen DH, Yang Y, Huang X. Targeting tumor-associated macrophages in cancer immunotherapy. *Cancers*. 2021;13(21). doi:10.3390/cancers13215318
69. Hu Z, Sui Q, Jin X, et al. IL6-STAT3-C/EBPβ-IL6 positive feedback loop in tumor-associated macrophages promotes the EMT and metastasis of lung adenocarcinoma. *J Exp Clin Cancer Res*. 2024;43(1):63. doi:10.1186/s13046-024-02989-x
70. You Y, Tian Z, Du Z, et al. M1-like tumor-associated macrophages cascade a mesenchymal/stem-like phenotype of oral squamous cell carcinoma via the IL6/Stat3/THBS1 feedback loop. *J Exp Clin Cancer Res*. 2022;41(1):10. doi:10.1186/s13046-021-02222-z
71. Williams L, Bradley L, Smith A, Foxwell B. Signal transducer and activator of transcription 3 is the dominant mediator of the anti-inflammatory effects of IL-10 in human macrophages. *J Immunol*. 2004;172(1):567–576.
72. Wan S, Zhao E, Kryczek I, et al. Tumor-associated macrophages produce interleukin 6 and signal via STAT3 to promote expansion of human hepatocellular carcinoma stem cells. *Gastroenterology*. 2014;147(6):1393–1404. doi:10.1053/j.gastro.2014.08.039
73. Calvier L, Chouvarine P, Legchenko E, et al. PPARγ links BMP2 and TGFβ1 pathways in vascular smooth muscle cells, regulating cell proliferation and glucose metabolism. *Cell Metab*. 2017;25(5). doi:10.1016/j.cmet.2017.03.011
74. Tseng V, Sutliff RL, Hart CM. Redox biology of peroxisome proliferator-activated receptor-γ in pulmonary hypertension. *Antioxid Redox Signal*. 2019;31(12):874–897. doi:10.1089/ars.2018.7695
75. Zou Y, Watters A, Cheng N, et al. Polyunsaturated fatty acids from astrocytes activate PPARγ signaling in cancer cells to promote brain metastasis. *Cancer Discov*. 2019;9(12):1720–1735. doi:10.1158/2159-8290.CD-19-0270
76. Nie S, Shi Z, Shi M, et al. PPARγ/SOD2 protects against mitochondrial ROS-dependent apoptosis via inhibiting ATG4D-mediated mitophagy to promote pancreatic cancer proliferation. *Front Cell Dev Biol*. 2021;9:745554. doi:10.3389/fcell.2021.745554